9-4-2007

# Approximation of Reaction Heat Effects in Cylindrical Catalyst Particles with Internal Voids using CFD

M. Ertan Taskin

Anthony G. Dixon
*Worcester Polytechnic Institute*, agdixon@wpi.edu

E. Hugh Stitt

Michiel Nijemeisland

INTERNATIONAL JOURNAL OF CHEMICAL REACTOR ENGINEERING

*Volume* 5 2007 *Article* A41

# Approximation of Reaction Heat Effects in Cylindrical Catalyst Particles with Internal Voids Using CFD

M. Ertan Taskin* Anthony G. Dixon†

E. Hugh Stitt‡ Michiel Nijemeisland**

*Worcester Polytechnic Institute, ertan@wpi.edu

†Worcester Polytechnic Institute, agdixon@wpi.edu

‡Johnson Matthey, hugh.stitt@matthey.com

**Johnson Matthey, michiel.nijemeisland@matthey.com

ISSN 1542-6580

# Approximation of Reaction Heat Effects in Cylindrical Catalyst Particles with Internal Voids Using CFD

M. Ertan Taskin, Anthony G. Dixon, E. Hugh Stitt, and Michiel Nijemeisland

## Abstract

Steam reforming reaction heat effects were implemented in CFD simulations of different packed tube models of 1-hole and 4-hole cylinders. A computationally less expensive 120° wall segment approach was utilized for the simulations in this study. Heat effects of the reactions were introduced by heat generation/consumption terms in the catalyst particles considering suitable reaction kinetics proposed in the literature. Due to strong diffusion limitations the activity of the catalyst particles is confined to a thin layer at the particle surface. Therefore, the energetic effects of the reactions were restricted to the outer 5% of the particle dimension by a user-defined code. The selection of the correct active region was verified for both the particle external and internal–hole surfaces. Simulation results of the reaction heat effects were qualitatively and quantitatively compared to cold flow cases where there were no heat effects but only tube wall heat transfer. Due to the endothermic nature of the reactions, relatively lower temperature fields were observed when the heat effects were introduced, where the positions of the solid particles play an important role. The implications of introducing the detailed reaction heat effects were emphasized in the development of suitable packed tube models.

**KEYWORDS:** Computational Fluid Dynamics, catalysts, heat transfer, fixed beds, steam reforming

# 1. INTRODUCTION

Packed tubes are extensively-used catalytic reactors in a wide variety of chemical processes. Multitubular narrow packed tubes are frequently the first choice for gas phase reactions with strong heat effects such as steam reforming or ethylene epoxidation. These packed tubes usually have a low tube-to-particle diameter ratio (N) since large particles must be used to reduce pressure drop at the high industrial flow rates, while the tube diameter is relatively small due to the need to transfer heat radially in or out of the tubes. Typical values of N are in the range 3 – 8, and in this range the tube transport properties are dominated by wall effects, which make reliable prediction of heat transfer rates quite a demanding task.

Steam reforming, in which highly endothermic reactions take place, is a widely-used chemical process for creating synthesis gas, which is a mixture of hydrogen gas and carbon monoxide. Sometimes the creation of the synthesis gas is the primary goal, in for example the production of hydrogen. Other times synthesis gas is produced as a precursor, mostly for hydrogen production for Fischer-Tropsch processes, or methanol, or ammonia synthesis (Stitt, 2005). A multitubular tube-and-shell design is generally selected for an industrial size steam reformer. The reactions take place in the catalyst-filled tubes while the necessary energy for the reactions is supplied from the shell side by a series of burners. Accurate prediction of the resulting tube wall temperatures and rates of heat transfer to the catalyst particles are essential for reliable reactor design.

Computational Fluid Dynamics (CFD) is a body of knowledge and techniques used to solve mathematical models of fluid dynamics on digital computers. CFD applications to reaction engineering are increasing rapidly with the development of high performance computers and advances in numerical techniques and algorithms (Ranade, 2002). CFD simulations may help to identify the possible causes of problems occurring in existing systems, and to provide useful insight to be used in design of experiments and scale up studies (Harris et al., 1996). Although CFD might not completely replace experimental work or standard modeling approaches currently used in the chemical engineering community (Kuipers and Van Swaaij, 1998), its great potential may be used to improve the available reactor modeling strategies, provided that proper validation against experimental results is carried out (e.g. Nijemeisland and Dixon, 2001).

Applications of CFD to packed tubes have recently been reviewed (Dixon et al., 2006). A major use of CFD is to obtain information regarding transport in the geometrically complex structure of the packed tubes without any simplifications such as the use of an effective porous medium and lumped parameters. Thus, by considering the detailed packing structures, interstitial flow, species and temperature fields can be obtained by solving equations based on the conservation laws of mass, momentum, and energy. Packed tube modeling by CFD techniques can be handled by automata-based simulation methods such as the Lattice Boltzmann Method (LBM), or based on the finite element /volume (FE/FV) solution of the continuum equations. Both techniques have been extensively applied to the flow field simulations, whereas, heat transfer simulations were mainly done by the finite element/volume methods. Although the LBM has not yet been successful in including heat transfer, it has been extended to chemical reaction in order to generate correlations between experimentally determined chemical conversion data and the LBM predicted flow fields, by Yuen at al. (2003) and Sullivan et al. (2005). To include flow, heat transfer and reaction simultaneously, commercial CFD codes using the FE/FV methods such as FLUENT and CFX have been used by our group and several others.

In addition to using CFD to obtain understanding and information about the transport processes in a packed tube of inert particles (Nijemeisland and Dixon, 2004), it is also desirable to simulate tube behavior with active catalyst particles. These simulations allow the assessment of the effects of different catalyst particle shapes and structures on the reactor performance, at a detailed level. Initially, it was anticipated that the difficulty and computational expense of carrying out 3D-simulations of diffusion, conduction and reaction inside catalyst pellets, coupled to a 3D external flow field, would be considerable. In addition, a straight-forward implementation did not appear possible as the particles were modeled as solid regions for conjugate heat transfer calculations with no flow, and equations for species transport were not available in solid regions. For these reasons we have looked for an alternative approach to the representation of heterogeneous reactions in packed tubes. Recently, we have been able to develop an approach to allow the simulation of species, energy and reaction inside catalyst particles in a CFD code, but the computational cost is, as expected, extremely high. Therefore, there is still a considerable benefit to an approximate approach that captures the main heat effects of the reactions.

As a first approach to including the reaction heat effects, we implemented user-defined code in the FLUENT CFD code to calculate temperature-dependent heat sinks/sources in the solid particle regions, for the steam reforming reactions. The strongly-diffusion-limited reactions in the particles (Pedernera et al., 2003) were approximated by using a step change in species partial pressures, so that the species were at the fluid composition in a thin region near the surface of the particle, and zero further in the particle. A relatively short segment of the reactor tube was modeled, and compositions were not allowed to change in the fluid. Reaction rates were then evaluated inside each particle, at the specified species partial pressures and at the computed local temperature, and combined with heats of reaction to give position-dependent sinks/sources. This was initially carried out for spherical catalyst particles (Dixon et al., 2003) and then extended to solid equilateral cylinders, for which some very brief results were reported in Nijemeisland et al. (2004). The algorithm to compute the sources/sinks was relatively simple for spheres, but was more complex for cylinders, where problems with particle orientation arise. A further elaboration of the method for full cylinders has been given in Dixon et al. (2006).

In the present study, the development of the extended algorithm for the implementation of the reaction heat effects to cylindrical particles with internal voids is presented. Verification of the approach for "egg-shell" type catalysts is given. This allows reaction heat effects to be assessed for more realistic steam reforming catalysts, such as Raschig rings and multihole cylinders. Some simulation results are given to emphasize the importance of this approach for packed tube modeling.

## 2. SIMULATION MODEL DEVELOPMENT

CFD codes can numerically solve the flow, species and energy balances in complicated flow geometries such as packed tubes. The basic equations used for the conservation of mass, momentum and energy are solved on the computational domain which is made up of a large number of control volumes, by discretizing them. At the time of writing, commercial CFD codes such as FLUENT are set up to solve all the basic equations in the fluid domain. In solid domains, by which the catalyst particles are defined, only the energy equation can be solved for conjugate heat transfer problems. Species balances are not usually available in a solid domain, which precludes the direct solution of diffusion-reaction problems in catalyst particles, when modeled as solids.

### 2.1 Model Geometries

The packed tube models were generated by the special geometry and mesh generation software GAMBIT 2.1.6 in 3D with a tetrahedral mesh structure and the simulations were carried out by the commercial CFD code FLUENT 6.2. The industrial flow conditions that were studied were obtained from a Johnson Matthey detailed reformer model of a methanol plant steam reformer with upwards flow, at typical operating conditions. The mass flow rate (or, equivalently, the superficial velocity) was kept constant for the two packing types in this work. Conditions were chosen to be those of the tube inlet, where temperature gradients are largest. The parameter values used in the simulations may be found in Dixon et al. (2003). Under these conditions, flow is fully turbulent. For that reason, to model these phenomena the k-ε turbulence scheme with the Renormalization Group (RNG) model was selected with a standard wall function approach.

Simulations of complete packed tubes rapidly become prohibitively expensive, especially if the solid particles are discretized, due to the need for a fine mesh (Dixon and Nijemeisland, 2001). A 120º wall segment (WS) model was previously developed for spherical packings with periodic top and bottom, and symmetric side conditions (Nijemeisland and Dixon, 2004). The wall segment approach resulted in computationally less expensive simulations and was extended to cylindrical packings (Nijemeisland et al., 2004) and was verified as a suitable approach to focus on a test particle in the near wall region (Taskin et al., 2007). The WS approach allowed detailed local analysis of the narrow packed tubes to investigate the transport properties at the tube wall, where the steepest gradients appear.

The WS models shown in Figure 1, with 1-hole cylinders and 4-hole cylinders, were used in the present study to illustrate the application of the reaction heat effects. Twelve equilateral cylinder catalyst particles with a size of 0.0254 m were placed at the same positions for both models. The dimension of the internal voids was also the same for each model, with a diameter of 0.0073 m. The test particle in the middle row of the three axial rows of

particles, and located tangentially near the center of the segment model was the only particle completely in the segment. The other particles in the geometries were not entirely in the wall segment models, and they were placed accordingly to provide typical surroundings for the test particle in the 120º bed segment with two complete axial layers of particles and translational periodic boundary conditions at the inlet and outlet. The model height was 0.0508 m. and the overall bed voidage was obtained to be 0.54 for the 1-hole cylinders model, and 0.66 for the 4-hole cylinders model.

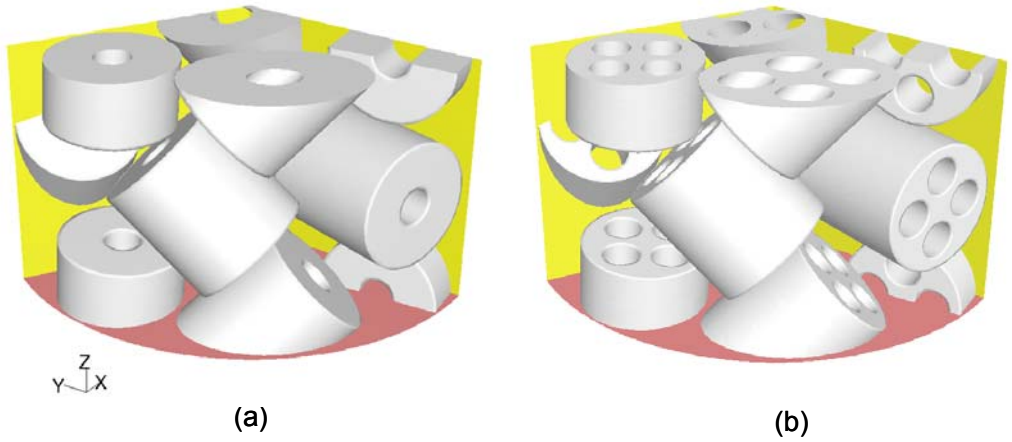


Figure 1. 3D views of (a) 1-hole cylinders and (b) 4-hole cylinders WS models

The temperature field was treated as non-periodic in the models because the gas was heated up as it passed through the segment. The isothermal periodic flow results were utilized as the flow field for the thermal solution since the temperature-dependence of the gas properties was not expected to strongly influence flow at the extremely high industrial flow rate simulated here. A uniform inlet temperature was specified, and to overcome the thermal entry effects, the models were virtually "stacked" by setting the outlet conditions of one stage as inlet conditions for the next stage. As a result developed temperature fields were obtained for models. All the heat transfer results presented here are for the third segment in the stack.

Due to the endothermic nature of the steam reforming reactions, in industry energy must be supplied from the outside burners to the tubes, mainly by radiation. Therefore, a constant heat flux boundary condition at the tube wall was selected for the runs. The same inlet temperature was set both for the fluid phase and for the bottom particle surfaces, for the first stage. Further details of the model geometry, mesh verification, model validations etc. are given in our prior publications. Our focus here is on the new developments that relate to the methodology of approximating the reaction heat effects.

## 2.2 Steam Reforming Heat Effects

Steam reforming kinetics have been determined by Xu and Froment (1989) and were implemented in a two-dimensional heterogeneous model of a reactor tube by Pedernera et al. (2003), and in a pseudohomogeneous model for a tubular membrane reactor by Gallucci et al. (2004), among others. For the present work, heat generation/consumption in the catalyst particles was simulated using reaction rates given by the kinetic model proposed by Hou and Hughes (2001) for methane steam reforming over a $Ni/\alpha Al_2O_3$ catalyst, as this catalyst formulation corresponded to the multihole particles that are the focus of the present study. This model is based on the steam reforming catalyst produced by Johnson Matthey Catalysts. The authors considered six possible reaction mechanisms, and they derived the intrinsic rate equations by the Langmuir-Hinshelwood-Hougen-Watson (LHHW) approach and Freundlich's adsorption concept. Five mechanisms were rejected by the model discrimination method, and the rate expressions were created for the remaining one utilizing only three main reactions among eleven base reactions. The three reactions were methane reforming to carbon monoxide (strongly endothermic), methane reforming to carbon dioxide (strongly endothermic) and the water-gas shift reaction (mildly exothermic). At the

lower temperatures of the reactor inlet, the dominant reaction is methane reforming to carbon dioxide. These reactions and the corresponding rate expressions are provided here in Table 1.

Table 1. Reactions and corresponding rate equations

| Reaction | Rate Equation | |
|---|---|---|
| $CH_4 + H_2O = CO + 3H_2$ | $r_1 = \dfrac{k_1\left(\dfrac{P_{CH_4}P_{H_2O}^{0.5}}{P_{H_2}^{1.25}}\right)\left(1-\dfrac{P_{CO}P_{H_2}^3}{K_{P1}P_{CH_4}P_{H_2O}}\right)}{\left(1+K_{CO}P_{CO}+K_H P_H^{0.5}+K_{H_2O}(P_{H_2O}/P_{H_2})\right)^2}$ | (1) |
| $CO + H_2O = CO_2 + H_2$ | $r_2 = \dfrac{k_2\left(\dfrac{P_{CO}P_{H_2O}^{0.5}}{P_{H_2}^{0.5}}\right)\left(1-\dfrac{P_{CO_2}P_{H_2}}{K_{P2}P_{CH_4}P_{H_2O}}\right)}{\left(1+K_{CO}P_{CO}+K_H P_H^{0.5}+K_{H_2O}(P_{H_2O}/P_{H_2})\right)^2}$ | (2) |
| $CH_4 + 2H_2O = CO_2 + 4H_2$ | $r_3 = \dfrac{k_3\left(\dfrac{P_{CH_4}P_{H_2O}}{P_{H_2}^{1.75}}\right)\left(1-\dfrac{P_{CO}P_{H_2}^4}{K_{P3}P_{CH_4}P_{H_2O}^2}\right)}{\left(1+K_{CO}P_{CO}+K_H P_H^{0.5}+K_{H_2O}(P_{H_2O}/P_{H_2})\right)^2}$ | (3) |

The reaction rate and equilibrium constants in the rate expressions were defined to be temperature-dependent through the Arrhenius and van't Hoff equations,

$$k_i = A_i \exp\left(-\frac{E_i}{RT}\right) \tag{4}$$

$$K_i = A(K_i)\exp\left(-\frac{\Delta H_{i,a}}{RT}\right) \tag{5}$$

The particular values of the activation energies, heats of adsorption and pre-exponential constants are available in Hou and Hughes (2001), and were used in the present study without alteration.

According to industrial observations, the activity is proportional to the geometric catalyst surface area. This is confirmed by the one-dimensional particle simulations of Pedernera et al. (2003), which suggest that reaction takes place within 3-5% of the particle radius from the surface. Therefore, the energetic effects of these reactions were considered to be confined to this region. In view of this information, the energetic effects of the reactions were defined for the outer 5% of the particle dimension by the user-defined volumetric heat generation terms. In other words, only the outer 5% of the particle dimension was considered as the active region of the particle. Before defining the heat effects by volumetric heat generation terms, the selection of the active region was verified by a separate user-defined code, which tested cells within each particle to see if they fell in the active region or not.

## 2.3 Verification of the Selection of Active Region

Prior to examining the cells within a particle, the position and orientation of the cylindrical particle had to be obtained. Further, the positions of the internal voids in the cylinder had also to be known. To get these, we made use of the procedure that was followed when the wall segment models were constructed. All particles were initially

placed at the coordinate axes origin, with the main cylinder axis aligned with the z-axis. A sequence of operations, rotations and translations, was then used to position each cylinder. An example is shown in Figure 2, for 4-hole cylinder particle number 1, the lower front particle in the wall segment. Note that wire frames of the previous positions are retained in each sketch for comparison. Each particle in the WS model had a similar sequence of operations.

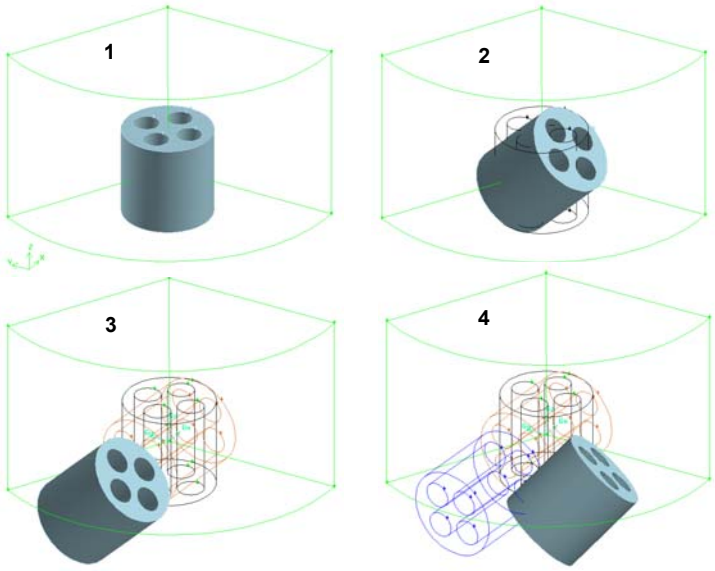


Figure 2. Sequence of transformations 1 → 2 → 3 → 4 to place bottom front 4-hole cylindrical particle.

The sequence shown in the example in Figure 2 consisted of a rotation of 45º around the positive x-axis (1 → 2), a translation of 0.03683 m in the negative x-direction (2 → 3), and a rotation of 40º around the positive z-axis (3 → 4). Each operation was represented by either a 3 × 3 matrix for a rotation, or a 3-vector for a translation. Since the initial position of the cylinder center point and the center point of the top surface were known, their images under the sequence of operations could be calculated, giving the coordinates of the center point and top center of the transformed particle. Similarly, the top center and middle center points for each internal void in the particle were easily calculated at the initial position, and then found for the particle voids under transformation. This information was then input to the algorithm for each of the particles.

The selection of the active region could then be tested for each particle. FLUENT defines an identification (ID) number for each surface and volume element in the geometry. Therefore each solid particle has a different ID number. As a first step, the user-defined code prepared for this purpose recognizes the particle with a specified number. Each solid catalyst particle is composed of many computational volumetric cells. The code stores the centroid coordinates of each cell. As an example, consider an arbitrary numerical cell which is illustrated by a blue dot as "Point ($x_p$, $y_p$, $z_p$)" in Figure 3. This schematic represents a sample solid cylindrical particle with the corresponding points necessary for the user-defined code. Additionally, the geometrical center coordinates of the solid particle, and the top-center coordinates of the top surface of the same solid particle are available from the procedure described above, and are given as input to the code. These points are shown by red dots as "Center ($x_c$, $y_c$, $z_c$)" and "Top ($x_t$, $y_t$, $z_t$)" respectively in Figure 3, along with the distances calculated from their coordinates.

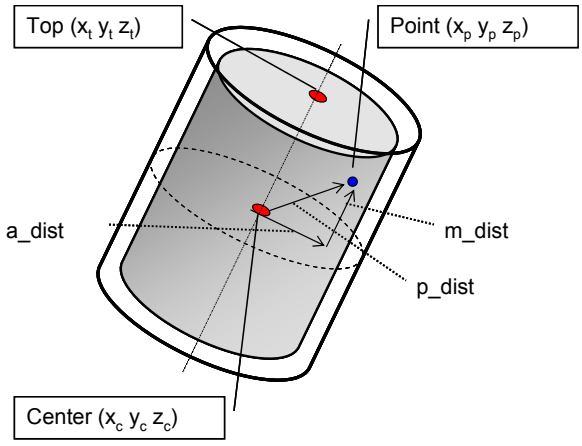


Figure 3. Sample solid particle and corresponding points for the verification of the selection of active region

The main idea of this verification study was to decide by a user-defined code whether a cell of interest will be located in the defined 5% active region or not (although the choice of 5% can easily be altered). The active region is shown by the non shaded area in Figure 3, and the corresponding algorithm for this code is given in Figure 4. To understand the relative location of each and every computational cell within the solid particle volume, three different distances were calculated. The distance between the "Center" and the "Point", denoted "p_dist", was calculated by Equation (6). The projection of this point onto the visual central plane of the particle perpendicular to its axis was used for the "m_dist" and "a_dist" calculations. The "m_dist", calculated according to Equation (7), is the distance between the "Point" and its corresponding projected point. The "a_dist" is calculated by the Pythagorean Theorem which gives the distance between the "Center" and the previous projected point.

$$p\_dist = \sqrt{(x_p - x_c)^2 + (y_p - y_c)^2 + (z_p - z_c)^2} \tag{6}$$

$$m\_dist = \left| \frac{(x_t - x_c)(x_p - x_c) + (y_t - y_c)(y_p - y_c) + (z_t - z_c)(z_p - z_c)}{\sqrt{(x_t - x_c)^2 + (y_t - y_c)^2 + (z_t - z_c)^2}} \right| \tag{7}$$

$$a\_dist = \sqrt{(p\_dist)^2 - (m\_dist)^2} \tag{8}$$

The "m_dist" and "a_dist" were used for understanding the relative position of the cell of interest. These two distances were compared with a cut-off parameter "$r_c$" which is defined as 95% of the cylindrical particle radius. Any point located inside the hypothetical cylinder volume with a radius of "$r_c$" corresponds to the inactive region of the catalyst particle. The comparison had to be done considering the radial and axial dimensions of the catalyst particle. So, when "a_dist" is compared with "$r_c$", the corresponding radial decision could be made. Similarly, the comparison of "m_dist" and "$r_c$" could lead to the axial decision. As given in the algorithm shown in Figure 4, both conditions had to be satisfied to decide on the inactive region.

The extension to consider internal voids followed the same principles. Additional "Center" and "Top" points were available which now lay on the axis of each circular void, and the distance of an arbitrary cell centroid from the axis, and thus from the surface of the void, could be calculated. Assuming that diffusion limitations would act in the same manner for all surfaces, whether on the particle external surface or on the internal void surface, the same cut-off value was used for all surfaces. So for a cell to be inactive its centroid had to be more than 5% of the particle radius from the flat top and bottom of the particle, the outer curved surface of the particle, and any internal surfaces of voids through the particle. This criterion is illustrated in the picture of active and inactive regions below.

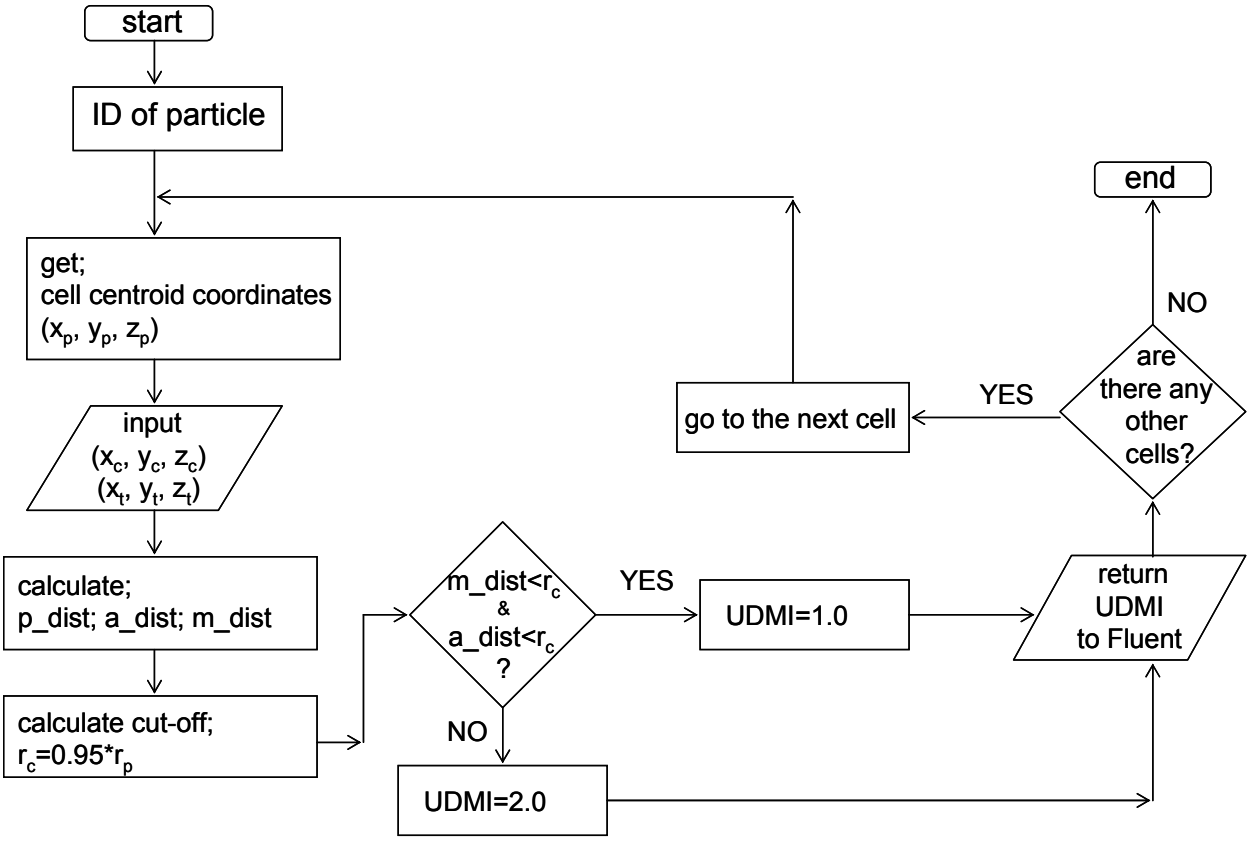


Figure 4. The algorithm for the verification of selection of active region for a full cylinder

The active and inactive regions were distinguished from each other by setting different user-defined-memory-indexes (UDMI) for the cells in these regions. These indexes were selected arbitrarily as 1.0 for the inactive region and as 2.0 for the active region, and were shown with different colors by FLUENT which made those regions visually distinguishable. The same procedure was applied for each cell of the solid particle by getting the corresponding cell centroid coordinates. After all the cells of one solid particle were covered, the same code was applied to the other solid particles.

The selection of the outer 5% dimension of the solid particles with the described code is given in Figure 5 for the bottom surfaces of the models which were shown by a light-red color in Figure 1. Also, an arbitrary section was enlarged to emphasize the active region selection better, considering the grid structures of the models. The active region was colored red, whereas the inactive region was colored green. The blue color represents the fluid section and the UDMI of 0.0 was set as default by FLUENT. The figure shows that the algorithm correctly selected the cells at the edges of the particles and did not select any fluid cells. The layers of selected cells appear somewhat ragged, and in some cases tetrahedra appear to have been selected that are not at the surface of a particle, and some tetrahedra that are at the surface of a particle appear not to have been selected. Examination of their centroid coordinates confirmed that the correct selection had been made. The apparent problem was due to the choice of a two-dimensional plane to show the results, the unstructured mesh, and the angle that a particle surface made with the viewing plane. In some cases the centroid of the tetrahedron was close enough to the surface for the cell to be selected, although the part of the cell that was intersected by the viewing plane appeared to be further from the particle surface. A similar explanation holds for the cells that look as if they are next to a surface, but which were not selected. The active region selection is based on the cell centroid coordinates of the 3D cells, and these cells were created with an unstructured grid. The code was also successful in selecting the related sections of the inner holes in the geometries.

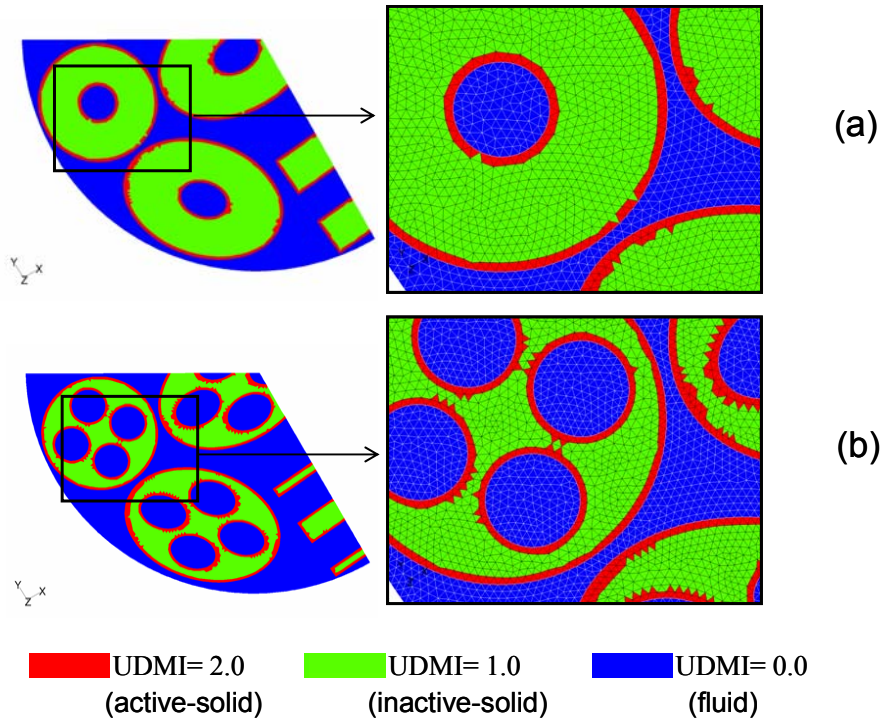


Figure 5. The bottom plane view of the selection of the active regions in (a) 1-hole cylinder, (b) 4-hole cylinder geometries

## 2.4 Introducing the Steam Reforming Heat Effects

The heat effects of the steam reforming reactions were introduced by a second user-defined code. The main structure of this code is similar to the one considered for the verification of the active region selection. The algorithm for this related code is given in Figure 6.

As a first step, the reaction rate and equilibrium constants, partial pressures and heats of reaction were input to the code. The code has 12 sub-codes corresponding to each of the 12 solid particles, and the above constants were just entered once in the beginning of the code before the sub-codes. FLUENT can provide a loop over the cells in a particular volume region. For a particular computational cell of a solid particle, the code recalls the cell temperature and centroid coordinates from FLUENT. Analogously to the verification part, the code calculates the relative position of the cell within the solid particle by equations (6), (7) and (8). The cut-off value was again calculated as 95% of the particle radius for the activity. In steam reforming reactions, temperatures are usually high and around 1000 K. Since the reaction rate expressions were not developed for low temperatures, it was decided to use a low-temperature cut-off of 500 K to prevent any possibility of anomalous results. If the cell temperature was less than the cut-off temperature, reaction was suppressed so that there would not be any heat effect. If the temperature was high enough, the algorithm would decide on the location of the cell by radial and axial comparison (for full cylinders) in the same way as expressed in the verification part. Additional tests were performed for particles with internal voids, again as described in the previous section. As a result of that decision, either the cell would be in the inactive region so that there would not be any heat effect, or the code calculated the temperature-dependent reaction rate constants and equilibrium constants by equations (4) and (5). The reaction rates given in Table 1 were calculated using these constants. The heat generated by the reactions was calculated by multiplying the reaction rates with the corresponding heat of reaction terms for all three reactions and summing them up. The units on all source terms must be in the form of heat generation-rate per volume (Fluent, 2005). Therefore, the heat generation term was multiplied by the solid density in order to obtain the source term “Q” according to Equation (9).

$$Q = \rho_s \sum_i r_i(-\Delta H_i) \tag{9}$$

The UDF code must return back to the main code the derivative of the source term with respect to the dependent variable of the transport equation, which is the temperature in this case. This term is used in the Finite Volume method to linearize the source term. Therefore, derivatives of all the temperature-dependent parameters of the source term were calculated in order to get the derivative of the source term. These expressions are extremely lengthy and will not be reproduced here. Once this term was returned back to the main code, the same procedure was applied for each cell of the solid particle. After all the cells of one solid particle were covered, the same procedure was applied to the other solid particles with different sub-codes.

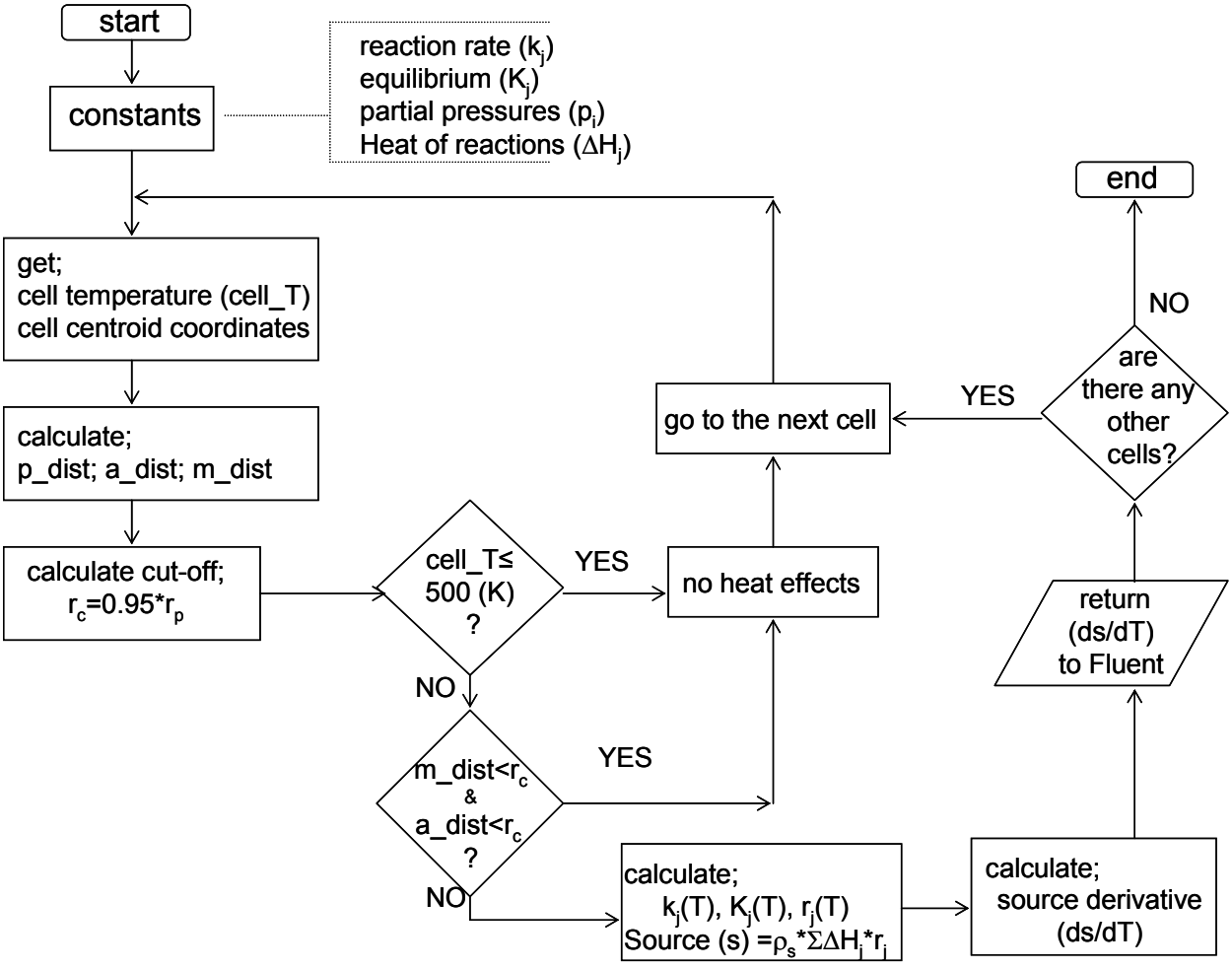


Figure 6. The algorithm for the application of reaction heat effects

## 3. RESULTS

In order to emphasize the influence of the application of the reaction heat effects, two different settings were considered separately; heat effects and no-heat effects. For the no-heat effects case, the code was not used and only the heat transfer from the tube wall was applied. Figure 7(a) and (c) show the temperature fields of the models obtained by the heat transfer simulations with no heat effects, whereas Figure 7(b) and (d) show the simulation results with heat effects of the reactions.

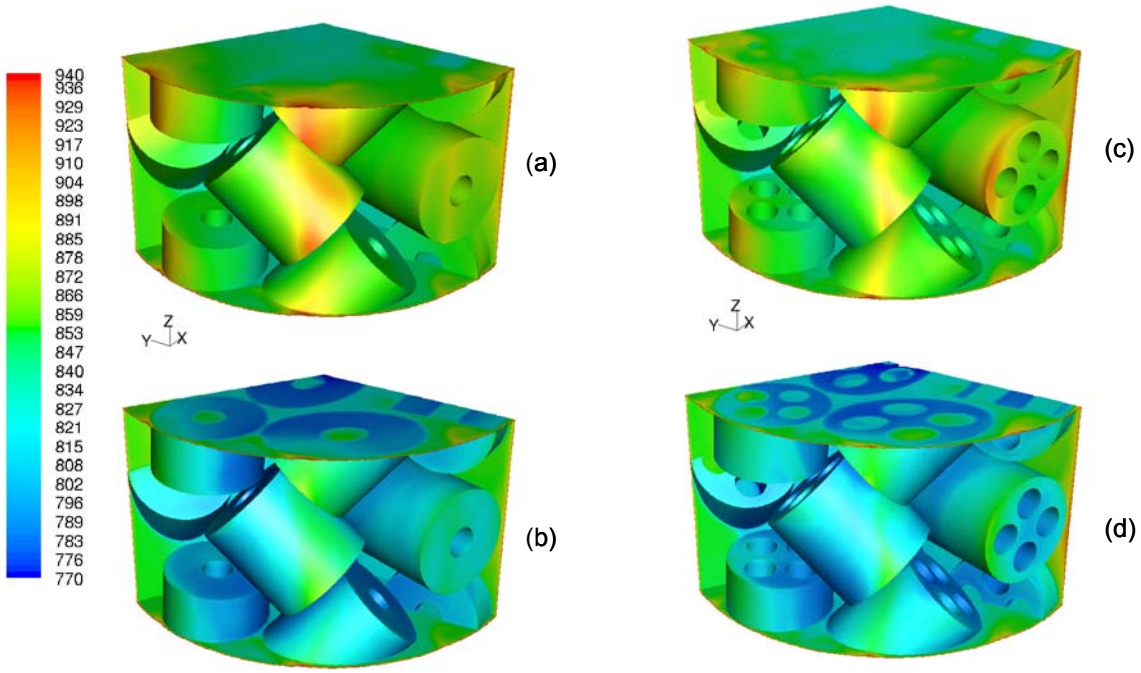


Figure 7. The temperature fields of (a) 1-hole cylinders model with no-heat effects, (b) 1-hole cylinders model with heat effects, (c) 4-hole cylinders model with no-heat effects, and (d) 4-hole cylinders model with heat effects

At a first glance, relatively cooler temperature fields were observed in Figure 7 when introducing the reaction heat effects. Since the code considers the reactions to be inside the solid particles only, and not in the fluid, the energy supplied from the outside of the wall was taken up by these solid particles as a result of the endothermic reactions, mainly reaction (3) the methane steam reforming to carbon dioxide. Therefore, the overall temperature field must be cooler in the case of reaction heat effects. When Figure 7(a) and (b) were compared, the cooler and hotter spots can be noticed at the same places on the 1-hole cylinders model in both figures. This means that the energy transferred from the wall was taken up by the particles in a uniform proportion. Actually, this was not surprising, because the activity was set as symmetric and uniform by confining it to the outer shell of the particles. Similar arguments could be made for the 4-hole cylinders model by looking at Figures 7(c) and (d). The particle temperatures were considerably lower than the fluid temperature in the case of reaction heat effects present, shown in Figure 7(b) and (d). As a result of that, at the top planes the particles were easily distinguishable from the fluid, whereas it was not so in Figure 7(a) and (c). These observations illustrate the qualitative results of the influence of the reaction heat effects.

The influence of the reaction heat effects on the temperature fields of the models could be quantitatively understood by considering the radial temperature profiles. Radial temperature profiles were obtained by averaging the temperatures at various constant values of r, over (Z, Θ) surfaces, including both fluid and solid regions. Each surface was defined at a different radial position from the center of the tube to the tube wall, having the same height as the model in the axial direction. As was demonstrated previously (Taskin et al., 2007), in order to get rid of the possible effects of imposing the symmetric plane side conditions, the averaging was done over the middle 60º part of the segment models. Resultant radial temperature profiles were plotted for both models with and without heat effects as shown in Figure 8 where the x-axis is the corresponding radial position, and the y-axis is the temperature.

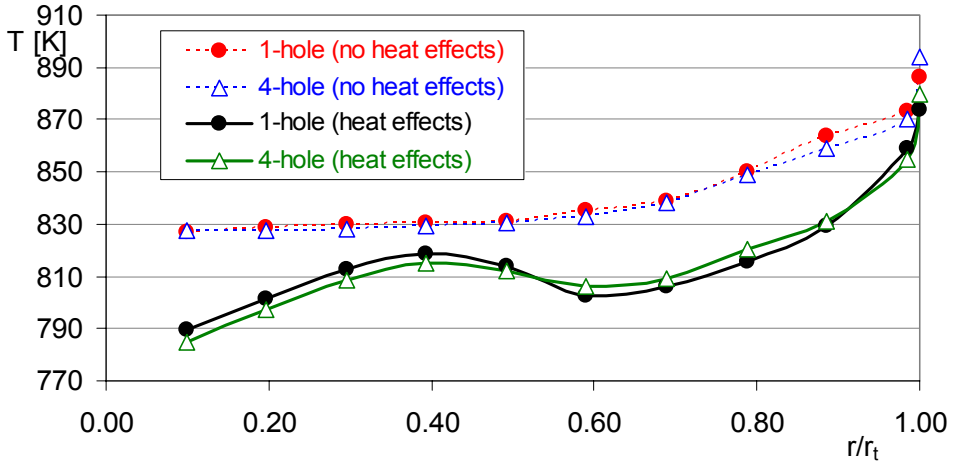


Figure 8. Radial temperature profiles of 1-hole and 4-hole cylinders models with and without heat effects

Radial temperature profiles for the simulations with no-heat effects were higher than the profiles of the simulations with heat effects. This quantitative observation matched with the qualitative overall temperature fields observation discussed above. The heat supplied from the wall kept the temperatures high near the wall, and then they start to decrease rapidly with distance from the wall, as expected. The main difference between the cases with and without heat effects was the appearance of the temperature "S" shape curve observed in the case with heat effects. Since there was heat consumption by the solid particles for the heat effects case, this "S" shape curve occurs due to the positions of the solid particles. The cases with no heat effects do not encounter the solid particles as a heat sink, so their temperature profiles were in the gradually decreasing form rather than being an "S" shape curve. The temperature profiles shown in Figure 8 do not include the sharp temperature increase across the boundary layer at the tube wall; average tube-side wall temperatures were approximately 1060 - 1080 K.

In order to see the radial temperature profiles of both cases and both models for solid and fluid domains individually, Figure 9 was generated where (a) presents the 1-hole cylinders model and (b) shows the 4-hole cylinders model. The temperature profiles in the no-heat effects cases were nearly the same for the solid and fluid domains, but they differ close to the wall. This is because in the steep temperature gradients near the wall the difference in thermal conductivity of the particles and gas is significant, whereas the effect is much less away from the wall and the high gradients. On the other hand, fluid and solid temperatures were quite different from each other for the heat effects cases and the profiles of the fluid domains were higher than the solid ones.

These are important observations in terms of the modeling approach in reaction engineering. One of the common packed tube models which is known as the "pseudohomogeneous" model, does not consider the presence of the solid phase and considers the bed as a single phase. Obviously, Figure 9 shows that, for heat transfer alone in a non-reacting tube this is a suitable approach, since there was no difference in temperature profiles in the solid and fluid. However, if the reaction heat effects are strong and have to be introduced, this model should not be selected.

Mears (1971) derived a well-known criterion for the neglect of the temperature difference between the particle and the fluid, based on a Taylor series expansion of the reaction rate about the bulk fluid temperature. The criterion for the rate not to deviate by more than 5% from the value calculated at the bulk fluid temperature was not satisfied for reaction (3) by a considerable margin for the conditions of the present simulations, confirming the conclusions drawn above from Figure 9. More recent criteria for the use of the pseudohomogeneous model (Dometti et al., 1999) are based on comparisons of qualitative features of the bifurcation diagrams of one-phase and two-phase models for exothermic reactions, and are thus not applicable to the endothermic reactions of the present study.

The radial temperature profiles computed from the fluid and solid volumes in the mesh and shown in Figure 8, exhibit a strong S-shape in the case of heat sinks present, which is not seen in the corresponding profiles for the individual phases shown in Figure 9. This observation may be explained by noting that in counting all the mesh cells, the fluid and solid temperatures are automatically weighted by the number of fluid and solid cells in the average. This is approximately equivalent to weighting the fluid and solid temperatures by the void fraction applicable at each radial position, according to the formula:

$$T(r) = \varepsilon(r)\,T_f(r) + (1-\varepsilon(r))\,T_s(r) \tag{10}$$

When the fluid and solid temperature profiles with heat effects in Figure 9 are added together according to Equation 10, using the void fraction profile obtained from the geometric model, the S-shaped profiles of Figure 8 are reproduced exactly. The curves presented in Figure 8 were calculated using Equation 10, and agree precisely with the symbols representing the values obtained from the CFD simulations.

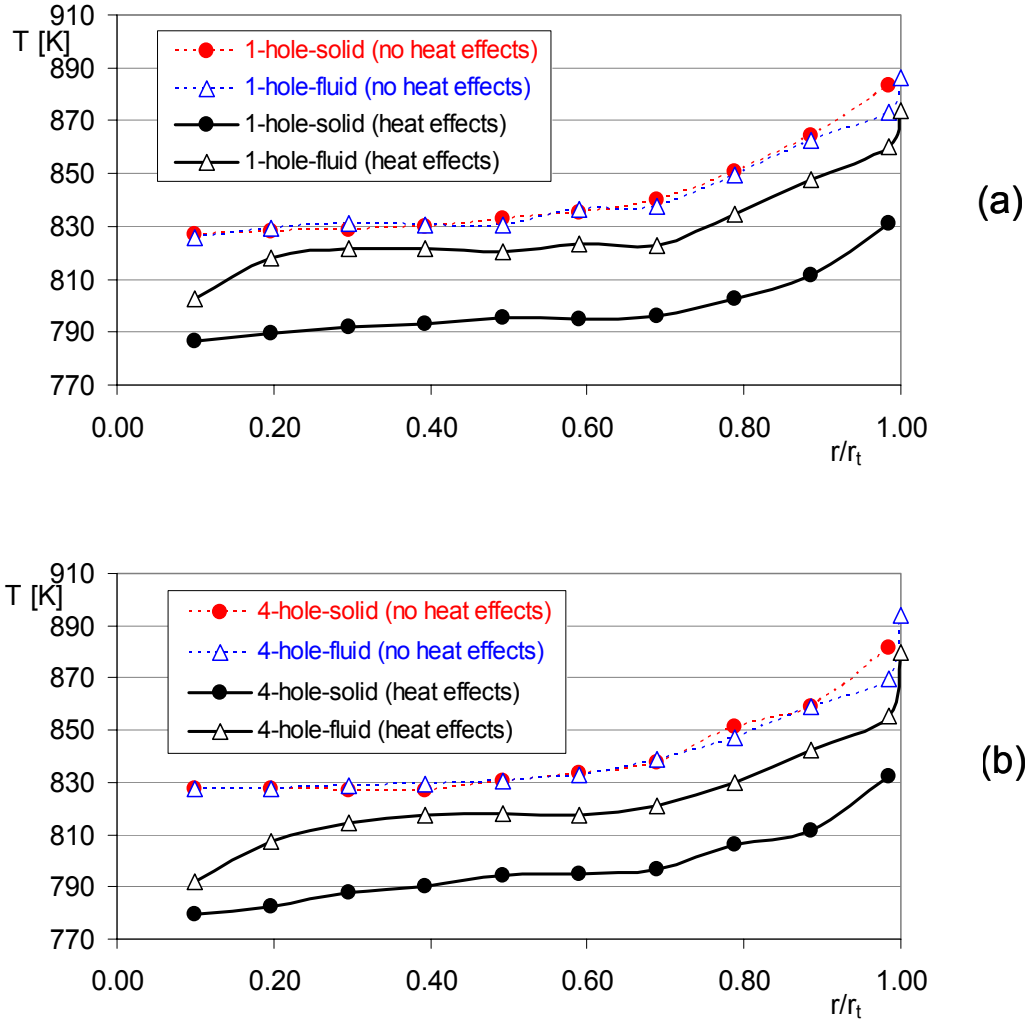


Figure 9. The radial temperature profiles of (a) 1-hole cylinders and (b) 4-hole cylinders models for separate solid and fluid domains

## 4. CONCLUSIONS

The steam reforming reaction heat effects were introduced by a used-defined code in the CFD simulations of two narrow packed tube models. For this purpose, the activity of the catalyst particles was defined, considering the industrial observations, to be confined to the 5% outer dimension of the particles. The selection of the 5% active region was verified with a different user-defined code. The heat effects were introduced by considering the heat of the reactions and reaction rates with the kinetic expressions which were previously developed in the literature.

The results of heat transfer simulations with and without heat effects were compared to each other for the studied models. The overall temperature fields and radial temperature profiles were generated for qualitative and quantitative comparisons. The introduction of heat effects caused lower temperature fields which were meaningful considering the endothermic nature of the reactions. It was observed that introducing the reaction heat effects causes the positions of the solid particles to play an important role in determining the temperature field of the models. For the no-heat effects case, the solid particles do not strongly influence the temperature fields. Therefore, the radial temperature profiles of the no-heat effects case did not show any significant difference when the solid and the fluid phases were separately plotted. Thus, this observation can be coupled with the basic idea behind the pseudohomogeneous type of packed tube modeling which does not account for the separate solid phase and utilizes lumped parameters instead of having separate parameters for fluid and solid phases.

The present paper illustrates the method devised to approximate the heat effects of reactions in an “egg-shell” type catalyst particle, using a fairly coarse unstructured grid in the particles. Our future work will implement mesh refinement using prism cells to resolve the boundary layer in the fluid outside the particle, as well as the shell inside the particle where source terms are active. Our preliminary calculations suggest that the difference between using the current UNS mesh in the particle and a suitably refined boundary layer mesh is approximately 3-4% for the particle heat uptake rate.

Regarding all the observations discussed above, there are valuable benefits of introducing the reaction heat effects in the near-surface regions of the particles to mimic the diffusion-limited reaction taking place in the solid particles in order to understand the temperature profiles in the packed tubes and to generate suitable models of them for the reactions with strong heat effects. A more extensive comparison of reaction heat effects in a wider variety of cylinder geometries with different operating conditions will be the focus of a future publication.

## NOTATION

| | |
|---|---|
| $A_j$ | pre-exponential constant for reaction j, same unit as $k_j$ |
| $A(K_i)$ | pre-exponential constant for adsorption constant of species i, same unit as $K_i$ |
| a_dist | distance between the “Center” and the projected point, Equation (8), m |
| ds/dT | derivative of the source term according to temperature |
| $E_j$ | activation energy of reaction j, J/mol |
| $\Delta H_j$ | heat of reaction j, J/mol |
| $\Delta H_{i,a}$ | heat of adsorption for species i, J/mol |
| $k_j$ | rate constant of reaction j, kmol/kg(cat.).s.$(kPa)^a$ |
| $K_{pi}$ | equilibrium constant for species i, $(kPa)^a$ |
| $K_i$ | adsorption constant for species i, $(kPa)^b$ |
| m_dist | distance between the “Point” and its corresponding projected point, Equation (7), m |
| p_dist | the distance between the “Center” and the “Point”, Equation (6), m |
| $P_i$ | partial pressure of species i, kPa |
| Q | volumetric heat generation rate, $W/m^3$(cat.) |
| r | radial coordinate, m |
| $r_c$ | cut-off value of radial coordinate, m |
| $r_j$ | rate of reaction j, kmol/kg(cat.).s |
| $r_p$ | particle radius, m |
| $r_t$ | tube radius, m |

| | |
|---|---|
| $r/r_t$ | dimensionless radial coordinate |
| R | gas constant, J/mol.K |
| T | temperature, K |
| UDMI | user defined memory index |
| $x_a,y_a,z_a$ | x, y, and z coordinates of point "a" |
| Z | axial coordinate, m |

Greek Letters

| | |
|---|---|
| $\varepsilon$ | turbulence dissipation rate, J/s |
| $\kappa$ | turbulent kinetic energy, J |
| $\rho_s$ | density of solid, kg(cat.)/$m^3$ |
| $\Theta$ | angular coordinate |

## REFERENCES

Dixon, A.G., Nijemeisland, M., "CFD as a Design Tool for Fixed-bed Reactors", Industrial & Engineering Chemistry Research, Vol. 40, 5246-5254 (2001).

Dixon, A. G., Nijemeisland, M., Stitt, E. H., "CFD Simulation of Reaction and Heat Transfer Near the Wall of a Fixed Bed", International Journal of Chemical Reactor Engineering, Vol. 1, A22, (2003).

Dixon, A. G., Nijemeisland, M., Stitt, E. H., "Packed Tubular Reactor Modelling and Catalyst Design Using Computational Fluid Dynamics", Advances in Chemical Engineering, Vol. 31, 307-389 (2006).

Dometti, S. M. S., Balakotaiah, V., West, D. H., "Analytical Criteria for Validity of Pseudohomogeneous Models of Packed-Bed Catalytic Reactors", Industrial & Engineering Chemistry Research, Vol. 38, 767-777 (1999).

Fluent 6.2 Users Guide, Fluent Inc., Lebanon, NH, (2005).

Gallucci, F., Paturzo, L., Basile, A., "A Simulation Study of the Steam Reforming of Methane in a Dense Tubular Membrane Reactor", International Journal of Hydrogen Energy, Vol. 29, 611-617, (2004).

Harris, C.K., Roekaerts, D, Rosendal, F.J.J, Buitendijk, F.G.J., Daskopoulos, Ph., Vreenegoor, A.J.N.,Wang, H. "Computational Fluid Dynamics for Chemical Reactor Engineering", Chemical Engineering Science, Vol. 51, 1569-1594, (1996).

Hou, K., Hughes, R., "The Kinetics of Methane Steam Reforming Over a Ni/α-$Al_2O$ Catalyst", Chemical Engineering Journal, Vol. 82, 311-328, (2001).

Kuijpers, J. A. M., van Swaaij, W.P.M, "Computational Fluid Dynamics Applied to Chemical Reaction Engineering", Advances in Chemical Engineering, Vol. 24, 227-328, (1998).

Mears, D. E., "Diagnostic Criteria for Heat Transport Limitations in Fixed Bed Reactors", Journal of Catalysis, vol. 20, 127-131, (1974).

Nijemeisland, M., Dixon, A.G., "Comparison of CFD Simulations to Experiment for Convective Heat Transfer in a Gas-solid Fixed Bed," Chem. Eng. J., Vol. 82, 231-246 (2001).

Nijemeisland, M., Dixon, A. G., "CFD Study of Fluid Flow and Wall Heat Transfer in a Fixed Bed of Spheres", American Institute of Chemical Engineers Journal, Vol. 50, 906-921, (2004).

Nijemeisland, M., Dixon, A. G., Stitt, E. H., "Catalyst Design by CFD for Heat Transfer and Reaction in Steam Reforming", Chemical Engineering Science, Vol. 59, 5185-5191, (2004).

Pedernera, M. N., Pina, J., Borio, D. O., Bucala, V., “Use of a Heterogeneous Two-dimensional Model to Improve the Primary Steam Reformer Performance”, Chemical Engineering Journal, Vol. 94, 29-40, (2003).

Ranade, V., “Computational Flow Modeling for Chemical Reactor Engineering”, Academic press, New York, (2002).

Stitt, E. H., “Reactor Technology for Syngas and Hydrogen. in Sustainable Strategies for the Upgrading of Natural Gas: Fundamentals, Challenges and Opportunities”, E. Derouane, V. Parmon, F. Lemos and F. Ramoa-Ribiero (eds.), NATO Science Series II, vol.191, Kluwer press, 185-216 (2005).

Sullivan, S.P., Sani, F.M., Johns, M. L., Gladden, L.F., “Simulation of Packed Bed Reactors Using Lattice Boltzmann Methods”, Chemical Engineering Science, Vol. 60, 3405-3418, (2005).

Taskin, M. E, Dixon, A. G., Stitt, E. H., “CFD Study of Fluid Flow and Heat Transfer in a Fixed Bed of Cylinders”, Numerical Heat Transfer, A: Applications, Vol. 52, 203-218 (2007).

Xu, J., Froment, G. F., “Methane Steam Reforming, Methanation and Water-gas Shift: I. Intrinsic Kinetics”, American Institute of Chemical Engineers Journal, Vol. 35, 88-96, (1989).

Yuen, E. H. L, Sederman, A. J., Sani, F., Alexander, P., Gladden, L. F., “Correlations Between Local Conversion and Hydrodynamics in a 3-D Fixed-Bed Esterification Process: An MRI and Lattice-Boltzmann Study”, Chemical Engineering Science, Vol. 58, 613-619, (2003).